

6 **Voltage imaging with ANNINE dyes and two-photon**
7 **microscopy of Purkinje dendrites in awake mice**
8

9
10 *Christopher J. Roome^{1*}, Bernd Kuhn^{1*}*
11

12
13 ¹OIST Graduate University, 1919-1 Tancha, Onna-son, Okinawa, Japan
14

15 *chris.roome@oist.jp, bkuhn@oist.jp
16

17 © 2019. This manuscript version is made available under the CC-BY-NC-ND 4.0
18 license <http://creativecommons.org/licenses/by-nc-nd/4.0/>
19

20 **Research Highlights**

- 21 • ANNINE dyes are purely electrochromic voltage sensitive dyes with linear,
22 nanosecond responses
23 • Red spectral edge excitation increases voltage sensitivity and reduces
24 phototoxicity and bleaching
25 • Dendritic voltage signals can be studied in awake animals using two-photon
26 imaging
27 • Voltage and calcium imaging, pharmacology, or electrical recordings can be
28 combined
29 • Subthreshold dendritic voltage signals reveal a 5 μ m basic unit of dendritic
30 computation

31

Abstract

32 Voltage imaging is the next generation of functional imaging in neuroscience. It promises to resolve
33 neuronal activity 10 to 100-times faster than calcium imaging and to report not only supra but also
34 subthreshold activity on a single cell or even subcellular level. Lately, several different voltage sensors and
35 imaging techniques were published which can achieve this. Here, we focus on a technique based on the
36 synthetic pure electrochromic voltage-sensitive dyes ANNINE-6 and ANNINE-6plus and the excitation of
37 this dye at the red spectral edge of absorption to maximize voltage sensitivity and minimize phototoxicity
38 and bleaching. Importantly, voltage imaging with ANNINE dyes can be done with one and two-photon
39 excitation. Two-photon microscopy allows in vivo, depth resolved imaging and line-scan recordings with
40 sub-millisecond temporal resolution. Interestingly for many future applications, the spectral characteristics
41 of ANNINE dyes allows simultaneous imaging with green indicators, like the genetically encoded calcium
42 indicator GCaMP6. We used this method to study supra and subthreshold dendritic voltage changes in
43 Purkinje neurons of awake mice. Simultaneously, we imaged dendritic calcium and recorded electrical
44 activity from the soma or locally applied drugs to show the full potential of the technique to study dendritic
45 integration in awake animals.

46

47

Introduction

48 Observing the brain at work on a cellular level is the dream of many neuroscientists. We would love to see
49 how neuronal activity triggered in the retina of our eye travels to the brain, how this activity is transmitted
50 from neuron to neuron, how this information of the outside world is processed and integrated in the
51 persistent neuronal network activity, and thereby update our brain-internal model of the outside world and
52 ourselves. This dream has already come true to some extent: there are several methods available to image
53 neuronal calcium activity of thousands of neurons and their processes in awake animals (Chen et al 2013)
54 with indicators which are based on a single, circularly permuted green fluorescent protein fused to a
55 calcium binding domain (Nakai et al 2001). However, to image the electrical activity in the mammalian
56 brain on a cellular or sub-cellular level is still a challenge. Electrical signals in the brain typically last only
57 one millisecond and therefore imaging must be even faster to capture such signals.

58 Voltage imaging was one of the first functional imaging methods developed, and the earliest reports go
59 back 50 years (Cohen et al 1974, Tasaki et al 1968). Using optimized synthetic voltage-sensitive dyes and
60 fast cameras, voltage was successfully imaged, for example, from neuronal networks in invertebrates
61 (Grinvald et al 1977, Senseman & Salzberg 1980), brain slices (Iijima et al 1996), brain modules in vivo
62 (Grinvald & Hildesheim 2004, Grinvald et al 1986), and single neurons and their compartments in brain

63 slices (Antic et al 1999, Antic & Zecevic 1995). However, voltage imaging in mammalian tissue in vivo
64 with single cell resolution or subcellular resolution failed because no method has been available for labeling
65 specific subgroups of neurons with synthetic dyes. If synthetic voltage-sensitive dyes are injected into tissue
66 or applied to the brain surface, they unspecifically label all cell surfaces in tissue, with axons, dendrites,
67 and astrocyte processes being the main plasma membrane contributors. Due to the dense packing of these
68 processes, the single structures cannot be optically resolved and only average membrane potential changes
69 can be measured.

70 Already 20 years ago, also genetically encoded voltage indicators were developed (Knöpfel 2012). Their
71 key advantage is that they can be targeted to specific cell types. Over the last few years their sensitivity and
72 temporal resolution have reached a very promising performance level. However, millisecond-resolution
73 single-cell-resolved voltage imaging with genetically encoded indicators in scattering tissue is still not
74 possible.

75 Recently, a promising hybrid approach was published, expressing a genetically encoded voltage sensor with
76 a domain to bind washed-in synthetic dye to enhance the fluorescence intensity (Abdelfattah et al 2019). It
77 allows to image populations of neurons in different types of tissue. This hybrid indicator system can so far
78 not be used with two-photon microscopy, but it has a great potential to do so in the near future.

79 Here, we first summarize our voltage imaging approach which is based on the synthetic voltage-sensitive
80 dyes ANNINE-6 and ANNINE-6plus. An in-depth primer of the method (Kuhn & Roome 2019) and
81 detailed protocols (Roome & Kuhn 2019) were published previously. In the second part, we give an
82 example of voltage imaging from dendrites of Purkinje neurons in awake mice (Roome & Kuhn 2018).

83

84 **Voltage sensing mechanism of ANNINE dyes**

85 About 20 years ago, we developed a novel family of synthetic voltage-sensitive dyes, in chemical terms
86 anellated hemicyanines, short ANNINEs (Hübener et al 2003, Kuhn & Fromherz 2003). The ANNINE
87 dyes, here represented by ANNINE-6 and ANNINE-6plus (Fromherz et al 2008) with a 6-ring chromophore
88 (Fig. 1a), are similar in most respects to other voltage-sensitive dyes like di-4-ANEPPS (Fig. 1a) (Fluhler
89 et al 1985) or RH-160 (Grinvald et al 1982). They have a hydrophobic tail group and a hydrophilic head
90 group. The headgroup of ANNINE-6 has a positive and a negative charge, while ANNINE-6plus has two
91 positive charges which makes it less hydrophobic. The amphiphilic design allows these dyes to bind to lipid
92 membranes (Fig. 1b). Their chromophore is formed by C and N atoms connected by conjugated single-
93 double bonds. As a result of this bonding type the electrons involved in the π -bond are delocalized and their

94 orbitals define the chromophore. These electrons are bound weakly and therefore the energy of a single
95 photon in the visible wavelength range, typically blue, is enough to excited one of the outermost electrons
96 from the ground state to an excited state. Importantly, the chromophore is elongated and asymmetric; aniline
97 forms one end, pyridinium the other. As a result of this asymmetry the center of charge of the delocalized
98 electrons is shifted towards aniline due to its higher electronegativity than pyridinium (Fig. 1c, center).
99 However, if one of the delocalized electrons gets excited by the absorption of a photon it is pulled toward
100 pyridinium and pushed away from aniline (Fig. 1c, center). So, a charge moves along the elongated axis of
101 the molecule.

102 The special feature of ANNINE dyes is that the chromophore is fully anellated. This makes the chemical
103 synthesis difficult, but the advantage is that the anellation prohibits conformational changes within the
104 chromophore due to rotation around single bonds or flipping at double bonds. ANNNE chromophores are
105 rigid. Conformational changes as rotations and flipping are associated with triplet state generation,
106 bleaching, and phototoxicity (Ephardt & Fromherz 1993, Röcker et al 1996). Conformational changes
107 might be also associated with movement of the dye at the membrane-water interface, resulting in a
108 fluorescence change that interferes with fluorescence changes due to the voltage sensing mechanism.

109 The design of the voltage-sensitive dye molecules with two carbohydrate chains and an elongated
110 chromophore ensures that the molecule axis is roughly aligned with the membrane normal. If the molecule
111 axis is aligned to the membrane normal and there is an electric field over the membrane, then the charge
112 movement within the molecule will be modulated by the external electric field over the membrane (Fig 1c,
113 left and right). For example, if the delocalized electron is shifted against the external electric field, less
114 energy is needed compared to no external electric field because the field pulls the electron (Fig. 1c left).
115 Therefore, the absorption spectrum shifts to lower energy, that is to longer wavelength. During the emission
116 process, the electron moves with the electric field and therefore loses energy. Hence, also the emission
117 spectrum will be shifted to lower energy. If the external electric field turns, as during an action potential,
118 the excitation and emission spectrum will be shifted to higher energy, that is shorter wavelength (Fig. 1c
119 right). If there are no other mechanisms of fluorescence change involved, the energy shift of both, the
120 excitation and emission spectrum, should be the same. Importantly, ANNINE dyes are so far the only
121 voltage-sensitive dyes which show this pure electrochromic effect where excitation and emission spectrum
122 are shifted by the same energy (Kuhn & Fromherz 2003). Additionally, ANNINE-6 exhibits the largest so
123 far measured charge shift in any voltage-sensitive dye. The charge shifts by 0.81 nm within the
124 chromophore (Kuhn & Fromherz 2003).

125 For voltage-sensitive dyes of this type only the spectra are shifted but the amplitude of the spectrum remains
126 unchanged. Unfortunately, the spectral shift is only very small (a few nanometer) as the external electric
127 field over the membrane and its changes are small in comparison with the electric fields within the dye
128 molecule. This contrasts with the widely used calcium indicators for which the amplitude is changing upon
129 binding of calcium ions while the spectral shape remains almost unchanged.

130 One advantage of ANNINE dyes is that the effect is purely based on the interaction of the charge in the
131 molecule and the electric field. As a result, the responses are linear and not influenced by diffusion
132 processes, conformational changes, or binding processes as for calcium indicators. Also, ANNINE dyes do
133 not move within the membrane and the chromophore conformation cannot change due to the anellation.
134 Other voltage-sensitive dyes move and can change their confirmation which influences their fluorescence.
135 Also, as the voltage-sensing mechanism is purely based on the interaction of a charge with an electric field,
136 the so-called molecular Stark effect (Kuhn & Fromherz 2003, Stark 1914), voltage imaging with ANNINE
137 dyes is independent of the membrane composition which makes the ANNINE dyes applicable in very
138 different tissue. Another advantage of using a pure molecular Stark-shift probe is that the responses are
139 almost instantaneous. For example, ANNINE-6 was used to resolve membrane voltage changes on a
140 nanosecond time scale (Frey et al 2006).

141

142 **Voltage imaging with ANNINE dyes**

143 Detectors, like camera sensors or photomultiplier tubes detect changes in fluorescence intensity. To convert
144 the spectral shift of the voltage-sensitive dyes into a measurable intensity change, spectral band pass filters
145 for excitation and emission are used. Here, as an example, we show the excitation spectrum of ANNINE-6
146 labeling the outer leaflet of the plasma membrane at resting potential (Fig. 2a, black spectrum). If the
147 voltage changes by 100 mV, the excitation spectrum shifts by about 3 nm (Fig. 2a, red spectrum). The
148 difference between two spectra is called the fluorescence change ΔF (Fig. 2b). The fluorescence change
149 normalized with the fluorescence spectrum results in the relative fluorescence change (Fig. 2c). Simplified,
150 there are two basic strategies to optimize the voltage signal, differing in the excitation light source.

151 If a white light source with the overall intensity distributed over a wide spectral range, such as a Xe-arc or
152 halogen lamp, and a band pass filter is used for excitation, it is best to choose the excitation filter so that at
153 the steepest slope of the spectrum is excited (Fig. 2a-c, blue arrows). Whenever the spectrum is shifted, this
154 will result in the largest signal, that is the largest fluorescence change (in this case, a decrease in intensity).
155 However, the sensitivity is relatively low and, therefore, many photons are needed to detect a signal. A

156 signal can only be detected if it overcomes the noise intrinsic to any optical measurement. Importantly, the
157 number of generated photons is proportional to phototoxicity caused by the excited dye. This is typically
158 not a problem for bulk loaded tissue but hampers recordings from fine structures as dendrites or axons.

159 The second strategy is to use a light source with almost unlimited intensity, i.e. lasers, for excitation and to
160 optimize the relative fluorescence change (Kuhn et al 2004). As the relative fluorescence change is
161 normalized to the number of detected photons, it is proportional to information about the voltage change
162 gained per detected photon. In this case it is best to excite at the spectral edge (Fig. 2a-c, black arrow) where
163 the relative fluorescence change is largest. However, the excitation spectrum corresponding to the excitation
164 probability is here very low (only a few % of the maximum) and, therefore, a white light source, e.g. Xe-
165 arc or halogen lamp, for excitation has insufficient intensity to generate a fluorescence intensity which
166 overcomes the photon shot-noise. This problem can be overcome by using lasers to excite. So, a very high
167 excitation intensity is required to achieve a useful fluorescence intensity, but at the spectral edge the
168 fluorescence change will be large as the relative fluorescence change is large. Important to note is that light
169 by itself is not harmful to tissue if it is not absorbed. Using high excitation intensity at the red spectral edge
170 is thus within a range that does not disturb or damage the tissue. With excitation at the red spectral edge of
171 the absorption spectrum, ANNINE-6 achieves a sensitivity of about 50% per 100 mV voltage change.
172 Additionally, bleaching or phototoxic effects are neglectable due to the low number of excited dye
173 molecules necessary to achieve a large optical signal for a voltage change. Additionally and for all
174 fluorescent molecules, it can be assumed that excitation at the red spectral edge of absorption is less harmful
175 as the smallest amount of energy is absorbed to generate an electronically excited state (Kuhn & Roome
176 2019).

177 Summarizing, the strategy for optimizing voltage imaging depends on the light source available. White
178 light sources such as Xe-arc lamps or halogen lamps are typically very stable light sources but only achieve
179 a limited relative fluorescence change. Alternatively, with lasers, high sensitivities can be achieved, but
180 some lasers tend to be less stable than white light sources and, for wide field excitation the speckle pattern,
181 resulting from the coherence of the laser light, hampers their applicability. For wide field imaging with
182 bright signals, both strategies work. However, for voltage imaging of fine structures, where bleaching and
183 phototoxicity affect the experiments, excitation with lasers at the red spectral edge of absorption becomes
184 crucial. Bright LED light sources, if available with a spectrum in the range between the steepest slope and
185 the spectral edge of the excitation spectrum, might bridge these two strategies

186 Labeling with synthetic voltage-sensitive dyes can be achieved by bath application to cell cultures or
187 injection into tissue in vivo. If the dye is externally applied, it will bind to the outer leaflet of the lipid

188 bilayer membrane. A depolarization of the membrane results in a decrease of the fluorescence intensity.
189 The advantage of this approach is that the labeling is easy to achieve. The disadvantage is that all membrane
190 surfaces are labeled, including glia, so that it is typically not possible to extract signals from a single neuron.
191 Using this approach, ANNINE dyes can be used to measure, for example, voltage changes of single neurons
192 in cell cultures (Pages et al 2011) or average membrane voltage changes and oscillations in vivo (Kuhn et
193 al 2008).

194 If the voltage-sensitive dye is intracellularly applied the dye will label the inner leaflet of the lipid
195 membrane. As the orientation of the dye in respect to the electric field over the membrane is reversed in
196 comparison to the extracellular application, the signal turns: The intensity increases with a depolarization
197 of the cell. The filling of single cells is tedious but allows to image the voltage from dendrites and axons in
198 vitro and in vivo (Antic et al 1999, Antic & Zecevic 1995, Roome & Kuhn 2018).

199 In general, voltage-sensitive dyes can flip from one leaflet of the lipid bilayer to the other until an
200 equilibrium is reached based on statistics and the dye's charge. If the dye will be equally distributed on both
201 sides, the voltage signal disappears. If the dye has a net charge the signal might even turn. Interestingly,
202 ANNINE dyes barely flip and show a similar sensitivity even after 2 weeks in vivo when intracellularly
203 applied (Roome & Kuhn 2018). Also when extracellularly applied to HEK293 or primary cell cultures
204 ANNINE dyes barely flip or internalize allowing extended imaging sessions (Pages et al 2011).

205 Voltage imaging is typically performed with one-photon excitation and cameras detection. In this case,
206 huge numbers of photons can be detected reducing the relative photon noise (photon noise divided by the
207 average number of detected photons). However, in scattering tissue as in the mammalian brain the spatial
208 resolution is limited. Two-photon microscopy can partly overcome the scattering problem (Helmchen &
209 Denk 2005). Additionally, two-photon microscopy allows optical sectioning. Due to the sectioning, the
210 number of excited dye molecules and detected photons is typically orders of magnitudes lower than with
211 wide-field one-photon excitation and camera imaging. Therefore, the relative photon noise is much higher.
212 ANNINE dyes can be easily excited at the red spectral edge of absorption with confocal microscopy (Kuhn
213 et al 2004, Pages et al 2011) and with two-photon microscopy, where the sensitivity increases (Fig. 2d-h)
214 (Kuhn et al 2008, Kuhn et al 2004, Roome & Kuhn 2018).

215 Finally, ANNINE-6 dyes can be easily combined with green calcium indicators, like GCaMP, because of
216 their spectral properties. This compatibility will allow a wide range of novel experiments.

217 The applicability of ANNINE dyes in neuroscience was previously demonstrated in neuronal cell cultures
218 (Pages et al 2011), in bulk loaded tissue in anesthetized and awake animals (Kuhn et al 2008), and, recently,
219 to image voltage in the dendrites of single Purkinje neurons in awake mice (Roome & Kuhn 2018).

220 To give an example of the full potential of the technique, we focus in the following paragraphs on the
221 Purkinje dendrite experiments (Roome & Kuhn 2018). At first, we argue for the importance of studying
222 dendritic integration under fully physiological conditions and the difficulties faced to do so. Then, we
223 explain the experimental design to overcome these difficulties and summarize our findings.

224

225 **Why study dendritic integration with voltage imaging in awake animals?**

226 Dendritic information processing is fundamental to how neurons work, and consequently, to how we
227 perceive and interact with the world around us. The elaborate geometries of neuronal dendrites, their non-
228 linear electrical properties, and the distribution and strength of their varied synaptic inputs, enables neurons
229 to perform complex computations (Häusser et al 2000, Stuart & Spruston 2015). The computations
230 underlying how we respond to sensory input and learn to make controlled movements for example, is
231 thought to occur through rapid spatio-temporal decoding of signals generated at dendritic synapses of
232 individual neurons, at the scale of microns and milliseconds (London & Häusser 2005, Segev & London
233 2000).

234 Over 60 years of experimental and theoretical studies devoted to understanding dendritic function have
235 provided great insight into the complex processing that dendrites can perform (Stuart et al 2016). However,
236 due to technological limitations, most experiments have been performed in brain slices and therefore lack
237 the synaptic inputs that occur in awake behaving animals. These key components are essential for
238 understanding dendritic signal processing in living animals.

239 Dendritic signal processing in the intact brain remains elusive, especially when investigating how dendritic
240 input influences somatic activity (neuronal output), also known as ‘dendritic integration’. This is
241 predominantly due to the technical limitations of recording from soma and dendrites simultaneously in
242 awake animals.

243 A well-known example of dendritic integration involves action potential back-propagation, whereby a
244 somatic action potential signal propagates backwards into the dendrites (Waters et al 2003) (in addition to
245 forwards along the axon). In doing so, it is thought to communicate a message of successful somatic action
246 potential generation to active dendritic synapses, and thereby modulate synaptic plasticity through local
247 dendritic calcium influx. This form of dendritic processing occurs in several neuron types, including

248 neocortical pyramidal neurons, and has been well-studied in brain slices (Stuart & Sakmann 1994). Back-
249 propagating action potentials are thought a key mechanism underlying how we learn and build memories
250 (Svoboda et al 1999). Their function in the intact brain, however, is highly controversial, if or how back-
251 propagating action potentials contribute during learning and memory remains unknown.

252 Another important example of dendritic integration thought to occur in cerebellar Purkinje neurons is
253 coincidence detection, whereby temporally coincident synaptic input from two distinct excitatory synaptic
254 inputs, parallel fibers and climbing fibers, is thought to trigger a neuronal signal that modifies the strength
255 of parallel fiber input to Purkinje neuron synapses, through synaptic plasticity (Ito 2000, Wang et al 2000).

256 Electrical recording in vivo (Margrie et al 2002), and somatic whole-cell recording in particular (Petersen
257 2017), has provided many insights into how neurons behave in their natural environment. However,
258 electrical recording from neuronal dendrites in vivo is challenging, and is often limited to anaesthetized
259 animals (Smith et al 2013) or restricted to single dendritic processes with limited spatial resolution across
260 the neuron (Moore et al 2017). Importantly, although generally considered the current state-of-the-art, these
261 techniques do not allow voltage and calcium recording from the finest spiny dendritic processes, that
262 receive the majority of synaptic inputs.

263 On the other hand, optical functional imaging techniques in awake animals combining two-photon
264 microscopy (Denk et al 1990), chronic cranial windows (Holtmaat et al 2009) and genetically encoded
265 indicators (Chen et al 2013) provide high spatio-temporal resolution from spiny dendrites (Yang & Yuste
266 2017). However, these techniques typically only use calcium indicators, reporting supra-threshold dendritic
267 signals at a temporal resolution limited by second messenger and indicator dynamics.

268 Thus, despite its importance, recording rapid (~ 1ms) signals from fine (< 1 μ m) dendritic processes in
269 awake animals is not possible through conventional approaches. Novel optical recording techniques
270 designed to overcome these limitations have been eagerly anticipated. Specifically, high resolution spatio-
271 temporal mapping of dendritic signaling using simultaneous voltage and calcium imaging is essential for
272 investigating dendritic integration in awake animals.

273

274 **Simultaneous voltage and calcium imaging from dendrites and electrical somatic recording from** 275 **Purkinje neurons in awake mice**

276 By combining simultaneous sub-millisecond voltage and calcium two-photon imaging from spiny dendrites
277 with somatic electrical recording, we investigated dendritic processing of spontaneously active cerebellar
278 Purkinje neurons (PNs) in awake resting mice. These multidimensional dendritic-somatic recordings are

279 the first to be conducted in an awake animal, serving as an introduction to the much-anticipated field of
280 voltage imaging from neuronal dendrites in behaving animals.

281 Several experimental challenges had to be overcome to do the experiments (Fig. 3).

282 Chronic cranial windows have been instrumental in advancing in vivo optical imaging studies, permitting
283 long-term high-resolution imaging in various brain regions in awake animals, however it does not allow to
284 access the brain. Using a simple modification to the chronic cranial window technique we incorporated a
285 sterile silicone access port into the window (Fig. 3a) that permits long-term repeated physical and optical
286 access to the brain (Fig. 3b) (Roome & Kuhn 2014).

287 Filling single neurons with ANNINE-6plus turned out to be a real challenge. However, ANNINE-6plus
288 dissolves well in ethanol (Fig. 3c) and we used this ANNINE-6plus/ethanol solution to label individual
289 neurons in vivo under a two-photon microscope (Fig. 3d) by electroporation (Fig. 3e-h). After some
290 practice, the electroporation procedure is a reliable way to fill Purkinje neurons in vivo (Fig. 3i-k) and also
291 other neurons such as cortical pyramidal neurons (Fig. 3l).

292 The chronic cranial window with access port also allowed us to perform simultaneous electrophysiology or
293 pharmacological manipulations and optical imaging on awake mice over several weeks (Roome & Kuhn
294 2018). Since animals recover quickly from surgery and can be used repetitively for many weeks (until bone
295 regrowth obscures the window), behavioral training may be implemented. Perhaps equally important, the
296 total number of animals used in research is significantly reduced, while the information gained from a single
297 animal is dramatically increased.

298 We double-labelled single cerebellar Purkinje neurons with ANNINE-6plus and GCaMP6f for
299 simultaneous dendritic voltage and calcium imaging. To reduce phototoxicity and increase signal
300 amplitude, we excited at the red spectral edge of absorption (1020nm). Using line scans (position indicated
301 in Fig. 3k) at a temporal resolution of 2 kHz we simultaneously recorded voltage and calcium signals from
302 the PN spiny dendrites (Fig. 4a,b). Extracellular electrophysiology was performed at the labelled PN soma
303 to record somatic activity (Fig. 4c). Pharmacological manipulations were also used to identify the voltage
304 and calcium dendritic signals that we recorded and importantly, these dendritic recordings could be repeated
305 for up to two weeks in an awake mouse (Roome & Kuhn 2018, Roome & Kuhn 2019).

306 Our results confirmed many findings that were described previously only in brain slices, including highly
307 attenuated back-propagating action potentials in the PN dendrites (Roome & Kuhn 2018). Dendritic voltage
308 imaging revealed spatio-temporal dendritic signaling patterns in PNs that was far more complex, dynamic,
309 and fine scaled than previously anticipated, and surprisingly, even in resting animals. We observed discrete

310 1–2 ms suprathreshold voltage spikelets that invaded the distal spiny dendrites during dendritic complex
311 spike events (Fig. 4d). These spikelets and their calcium correlates are highly variable in number, timing
312 and most striking, in their spatial variability, such that the number of calcium spikelets generated by a single
313 climbing fiber input varied across different dendritic regions to produce fully spatially and temporally
314 graded calcium signals evoked by the formally assumed monolithic ('all-or-none') complex spike event
315 (Fig. 4d).

316 Dendritic voltage imaging also detected rapid subthreshold voltage signals evoked by parallel fiber synaptic
317 input for the first time in vivo (Fig. 5a, also visible in Fig. 4a). These events, we refer to as 'hotspots', were
318 localized to fine dendritic processes and had no corresponding calcium signal. Hotspots were partially
319 blocked by AMPA/kainate antagonist (CNQX) and by Na⁺ channel antagonist (lidocaine) and showed
320 regimes of linear and nonlinear relationship with the somatic simple spike firing rate (Fig. 5c-d) (Roome &
321 Kuhn 2018). It was surprising to find that hotspot synaptic EPSPs were remarkably fast (5–10 ms) and
322 localized to short (~5μm) dendritic segments, with a shorter apparent length constant than had been
323 predicted from computational modelling techniques (De Schutter & Bower 1994b, Roth & Häusser 2001).
324 It is worth noting however that the spatial extent of these signals agrees well with clustered co-activated
325 synaptic input observed in layer 2/3 pyramidal neurons in the cortex (Scholl et al 2017, Wilson et al 2016),
326 and supports theories for spatio-temporally clustered synaptic input and fine-scale (5-10 micrometer) units
327 of dendritic computation in vivo (Larkum & Nevian 2008, Wilms & Häusser 2015, Yasuda & Murakoshi
328 2011). It is likely that the EPSP length constant is modulated by intrinsic dendritic mechanisms (i.e. active
329 and passive channels) and/or coincident synaptic mechanisms, such as through feedforward inhibition via
330 molecular interneurons (De Schutter 1998, De Schutter & Bower 1994a, Mittmann et al 2005).

331 In addition to the well-known climbing fiber evoked dendritic calcium spikes, we also detected rare non-
332 climbing fiber evoked dendritic spikes that occurred following a sharp increase in hotspot activity in the
333 spiny dendrites (Fig. 5a and e). Unlike climbing fiber evoked dendritic spikes, dendritic spike events
334 generated a smaller localized elevation in dendritic calcium and with no associated somatic signal. Parallel
335 fiber evoked dendritic spikes had not previously been observed in vivo. PF evoked dendritic spike events
336 frequently follow climbing fiber evoked dendritic complex spike events, and thus contribute to the overall
337 dendritic calcium signal. Our findings indicate that a strong increase in parallel fiber input evoked by
338 sensory stimulation, for example, may function to enhance dendritic calcium influx if a coincident climbing
339 fiber-evoked event occurs. This form of dendritic coincidence detection of parallel fiber and climbing fiber
340 input is known to induce long-term depression (LTD) at PF-PN synapses (in brain slices) (Wang et al 2000)
341 and is thought a key mechanism underlying learning for the control of movements by the cerebellum.

342

343 **Acknowledgement**

344 The authors thank the Okinawa Institute of Science and Technology Graduate University for internal
345 funding.

346

347 **Author Contributions**

348 C.J.R. and B.K. wrote the manuscript.

349

350 **Conflict of Interest Statement**

351 The authors have no conflict of interest.

352 **References**

- 353 Abdelfattah AS, Kawashima T, Singh A, Novak O, Liu H, et al. 2019. Bright and photostable chemigenetic
354 indicators for extended in vivo voltage imaging. *Science* 365: 699-704
- 355 Antic S, Major G, Zecevic D. 1999. Fast optical recordings of membrane potential changes from dendrites
356 of pyramidal neurons. *J Neurophysiol* 82: 1615-21
- 357 Antic S, Zecevic D. 1995. Optical signals from neurons with internally applied voltage-sensitive dyes. *J*
358 *Neurosci* 15: 1392-405
- 359 Chen TW, Wardill TJ, Sun Y, Pulver SR, Renninger SL, et al. 2013. Ultrasensitive fluorescent proteins for
360 imaging neuronal activity. *Nature* 499: 295-300
- 361 Cohen LB, Salzberg BM, Davila HV, Ross WN, Landowne D, et al. 1974. Changes in axon fluorescence during
362 activity - Molecular probes of membrane potential. *J Membrane Biol* 19: 1-36
- 363 De Schutter E. 1998. Dendritic voltage and calcium-gated channels amplify the variability of postsynaptic
364 responses in a Purkinje cell model. *Journal of neurophysiology* 80: 504-19
- 365 De Schutter E, Bower JM. 1994a. An active membrane model of the cerebellar Purkinje cell II. Simulation
366 of synaptic responses. *Journal of neurophysiology* 71: 401-19
- 367 De Schutter E, Bower JM. 1994b. Simulated responses of cerebellar Purkinje cells are independent of the
368 dendritic location of granule cell synaptic inputs. *Proceedings of the National Academy of Sciences*
369 *of the United States of America* 91: 4736-40
- 370 Denk W, Strickler JH, Webb WW. 1990. Two-photon laser scanning fluorescence microscopy. *Science* 248:
371 73-6
- 372 Ephardt H, Fromherz P. 1993. Fluorescence of amphiphilic hemicyanine dyes without free double-bonds.
373 *J Phys Chem* 97: 4540-47
- 374 Fluhler E, Burnham VG, Loew LM. 1985. Spectra, membrane-binding, and potentiometric responses of
375 new charge shift probes. *Biochem* 24: 5749-55
- 376 Frey W, White JA, Price RO, Blackmore PF, Joshi RP, et al. 2006. Plasma membrane voltage changes during
377 nanosecond pulsed electric field exposure. *Biophys J* 90: 3608-15
- 378 Fromherz P, Hübener G, Kuhn B, Hinner MJ. 2008. ANNINE-6plus, a voltage-sensitive dye with good
379 solubility, strong membrane binding and high sensitivity. *Eur Biophys J Biophys* 37: 509-14
- 380 Grinvald A, Hildesheim R. 2004. VSDI: A new era in functional imaging of cortical dynamics. *Nat Rev*
381 *Neurosci* 5: 874-85
- 382 Grinvald A, Hildesheim R, Farber IC, Anglister L. 1982. Improved fluorescent probes for the measurement
383 of rapid changes in membrane potential. *Biophys J* 39: 301-08
- 384 Grinvald A, Lieke E, Frostig RD, Gilbert CD, Wiesel TN. 1986. Functional architecture of cortex revealed by
385 optical imaging of intrinsic signals. *Nature* 324: 361-4
- 386 Grinvald A, Salzberg BM, Cohen LB. 1977. Simultaneous recording from several neurones in an
387 invertebrate central nervous system. *Nature* 268: 140-2
- 388 Häusser M, Spruston N, Stuart GJ. 2000. Diversity and dynamics of dendritic signaling. *Science* 290: 739-
389 44
- 390 Helmchen F, Denk W. 2005. Deep tissue two-photon microscopy. *Nat Methods* 2: 932-40
- 391 Holtmaat A, Bonhoeffer T, Chow DK, Chuckowree J, De Paola V, et al. 2009. Long-term, high-resolution
392 imaging in the mouse neocortex through a chronic cranial window. *Nat Protoc* 4: 1128-44
- 393 Hübener G, Lambacher A, Fromherz P. 2003. Anellated hemicyanine dyes with large symmetrical
394 solvatochromism of absorption and fluorescence. *J Phys Chem B* 107: 7896-902
- 395 Iijima T, Witter MP, Ichikawa M, Tominaga T, Kajiwara R, Matsumoto G. 1996. Entorhinal-hippocampal
396 interactions revealed by real-time imaging. *Science* 272: 1176-9
- 397 Ito M. 2000. Mechanisms of motor learning in the cerebellum. *Brain Res* 886: 237-45

398 Knöpfel T. 2012. Genetically encoded optical indicators for the analysis of neuronal circuits. *Nat Rev*
399 *Neurosci* 13: 687-700

400 Kuhn B, Denk W, Bruno RM. 2008. In vivo two-photon voltage-sensitive dye imaging reveals top-down
401 control of cortical layers 1 and 2 during wakefulness. *Proc Natl Acad Sci U S A* 105: 7588-93

402 Kuhn B, Fromherz P. 2003. Anellated hemicyanine dyes in a neuron membrane: Molecular Stark effect
403 and optical voltage recording. *J Phys Chem B* 107: 7903-13

404 Kuhn B, Fromherz P, Denk W. 2004. High sensitivity of Stark-shift voltage-sensing dyes by one- or two-
405 photon excitation near the red spectral edge. *Biophys J* 87: 631-39

406 Kuhn B, Roome CJ. 2019. Primer to Voltage Imaging With ANNINE Dyes and Two-Photon Microscopy. *Front*
407 *Cell Neurosci* 13: 321

408 Larkum ME, Nevian T. 2008. Synaptic clustering by dendritic signalling mechanisms. *Curr Opin Neurobiol*
409 18: 321-31

410 London M, Häusser M. 2005. Dendritic computation. *Annual review of neuroscience* 28: 503-32

411 Margrie TW, Brecht M, Sakmann B. 2002. In vivo, low-resistance, whole-cell recordings from neurons in
412 the anaesthetized and awake mammalian brain. *Pflugers Arch* 444: 491-8

413 Mittmann W, Koch U, Häusser M. 2005. Feed-forward inhibition shapes the spike output of cerebellar
414 Purkinje cells. *J Physiol* 563: 369-78

415 Moore JJ, Ravassard PM, Ho D, Acharya L, Kees AL, et al. 2017. Dynamics of cortical dendritic membrane
416 potential and spikes in freely behaving rats. *Science* 355

417 Nakai J, Ohkura M, Imoto K. 2001. A high signal-to-noise Ca²⁺ probe composed of a single green fluorescent
418 protein. *Nat Biotechnol* 19: 137-41

419 Pages S, Cote D, De Koninck P. 2011. Optophysiological approach to resolve neuronal action potentials
420 with high spatial and temporal resolution in cultured neurons. *Front Cell Neurosci* 5: 20

421 Petersen CCH. 2017. Whole-Cell Recording of Neuronal Membrane Potential during Behavior. *Neuron* 95:
422 1266-81

423 Röcker C, Heilemann A, Fromherz P. 1996. Time-resolved fluorescence of a hemicyanine dye: Dynamics of
424 rotamerism and resolution. *J Phys Chem* 100: 12172-77

425 Roome CJ, Kuhn B. 2014. Chronic cranial window with access port for repeated cellular manipulations,
426 drug application, and electrophysiology. *Front Cell Neurosci* 8: 379

427 Roome CJ, Kuhn B. 2018. Simultaneous dendritic voltage and calcium imaging and somatic recording from
428 Purkinje neurons in awake mice. *Nat Commun* 9: 3388

429 Roome CJ, Kuhn B. 2019. Voltage imaging with ANNINE dyes and two-photon microscopy. In *Multiphoton*
430 *Microscopy*, ed. E Hartveit: Springer Nature (Neuromethods)

431 Roth A, Häusser M. 2001. Compartmental models of rat cerebellar Purkinje cells based on simultaneous
432 somatic and dendritic patch-clamp recordings. *J Physiol* 535: 445-72

433 Scholl B, Wilson DE, Fitzpatrick D. 2017. Local Order within Global Disorder: Synaptic Architecture of Visual
434 Space. *Neuron* 96: 1127-38 e4

435 Segev I, London M. 2000. Untangling dendrites with quantitative models. *Science* 290: 744-50

436 Senseman DM, Salzberg BM. 1980. Electrical activity in an exocrine gland: optical recording with a
437 potentiometric dye. *Science* 208: 1269-71

438 Smith SL, Smith IT, Branco T, Häusser M. 2013. Dendritic spikes enhance stimulus selectivity in cortical
439 neurons in vivo. *Nature* 503: 115-20

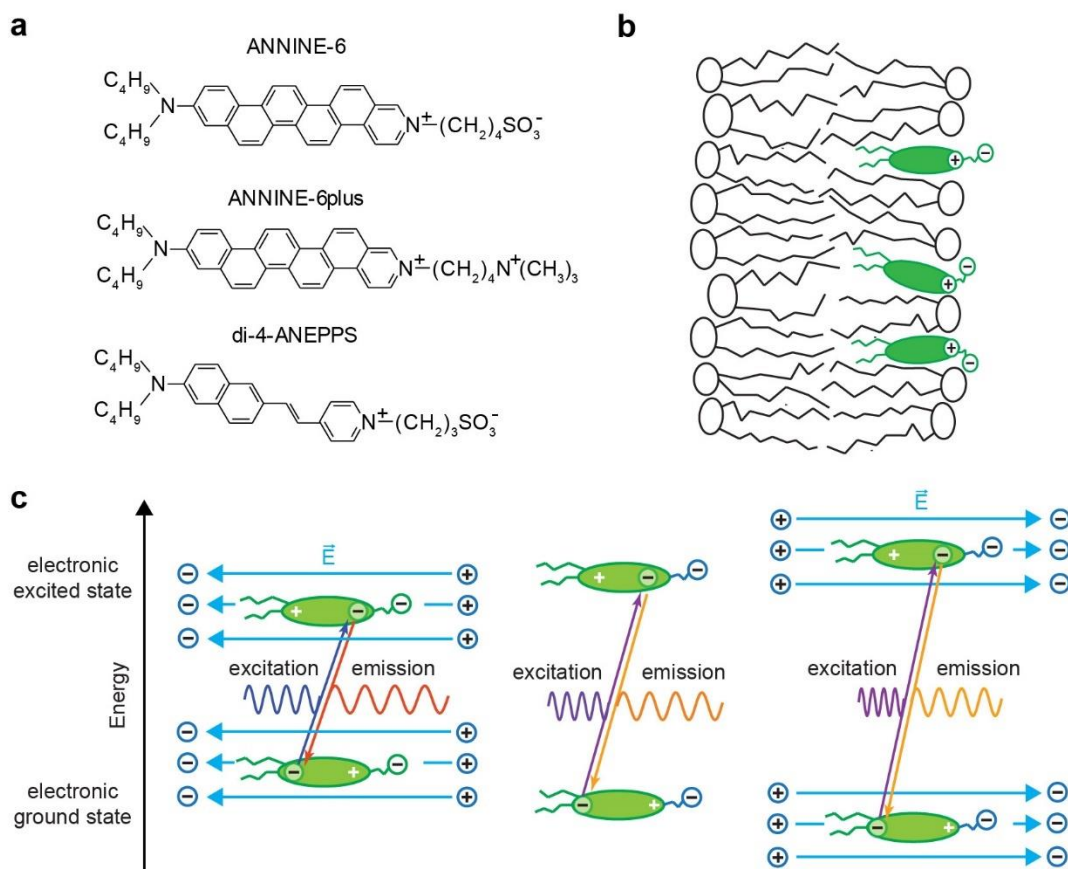
440 Stark J. 1914. Observations on the effect of the electrical field on spectral lines I Transverse effect. *Ann*
441 *Phys-Berlin* 43: 965-82

442 Stuart G, Spruston N, Häusser M. 2016. *Dendrites*. Oxford ;: Oxford University Press. xxi, 714 pages pp.

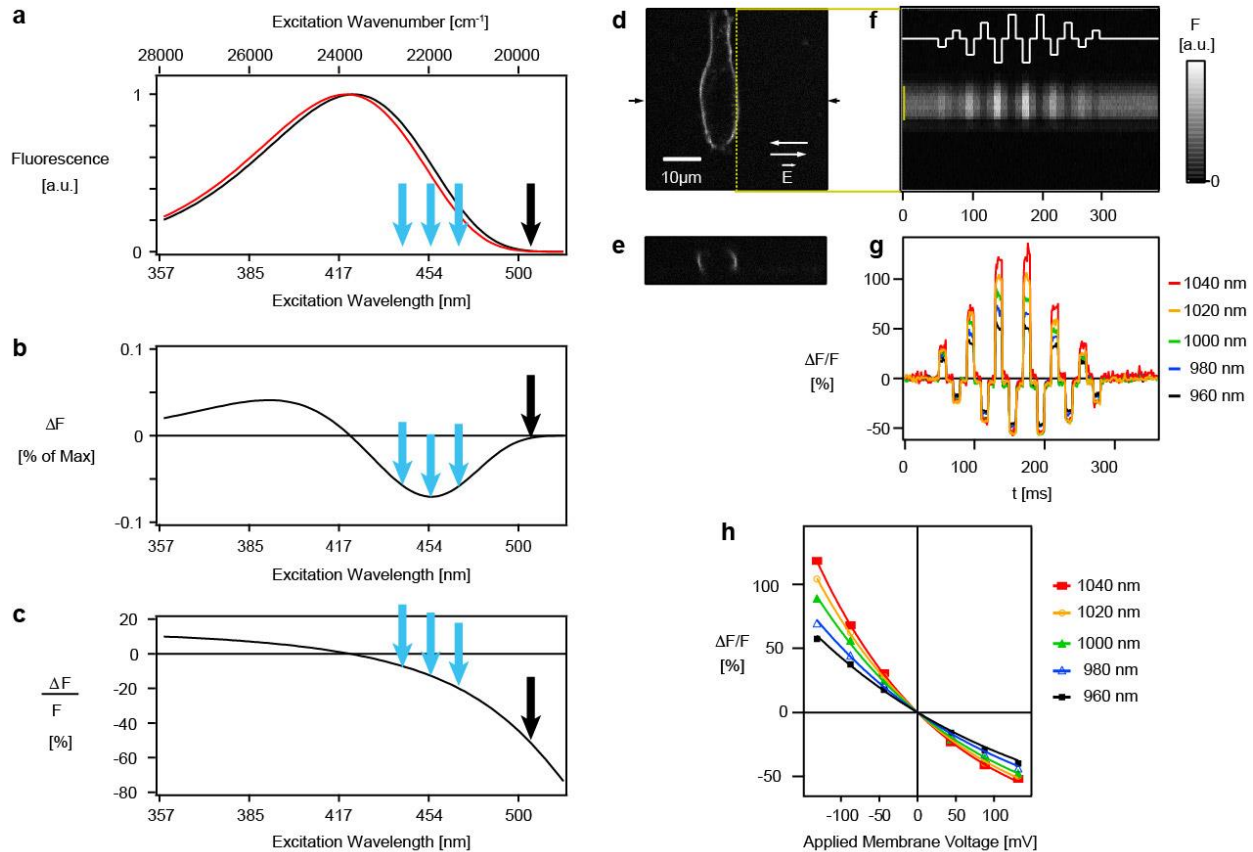
443 Stuart GJ, Sakmann B. 1994. Active propagation of somatic action potentials into neocortical pyramidal
444 cell dendrites. *Nature* 367: 69-72

445 Stuart GJ, Spruston N. 2015. Dendritic integration: 60 years of progress. *Nat Neurosci* 18: 1713-21

446 Svoboda K, Helmchen F, Denk W, Tank DW. 1999. Spread of dendritic excitation in layer 2/3 pyramidal
447 neurons in rat barrel cortex in vivo. *Nat Neurosci* 2: 65-73
448 Tasaki I, Watanabe A, Sandlin R, Carnay L. 1968. Changes in fluorescence, turbidity, and birefringence
449 associated with nerve excitation. *Proc Natl Acad Sci U S A* 61: 883-8
450 Wang SS-H, Denk W, Häusser M. 2000. Coincidence detection in single dendritic spines mediated by
451 calcium release. *Nat Neurosci* 3: 1266-73
452 Waters J, Larkum M, Sakmann B, Helmchen F. 2003. Supralinear Ca²⁺ influx into dendritic tufts of layer
453 2/3 neocortical pyramidal neurons in vitro and in vivo. *The Journal of neuroscience : the official*
454 *journal of the Society for Neuroscience* 23: 8558-67
455 Wilms CD, Häusser M. 2015. Reading out a spatiotemporal population code by imaging neighbouring
456 parallel fibre axons in vivo. *Nature communications* 6: 6464
457 Wilson DE, Whitney DE, Scholl B, Fitzpatrick D. 2016. Orientation selectivity and the functional clustering
458 of synaptic inputs in primary visual cortex. *Nat Neurosci* 19: 1003-9
459 Yang W, Yuste R. 2017. In vivo imaging of neural activity. *Nature methods* 14: 349-59
460 Yasuda R, Murakoshi H. 2011. The mechanisms underlying the spatial spreading of signaling activity. *Curr*
461 *Opin Neurobiol* 21: 313-21
462



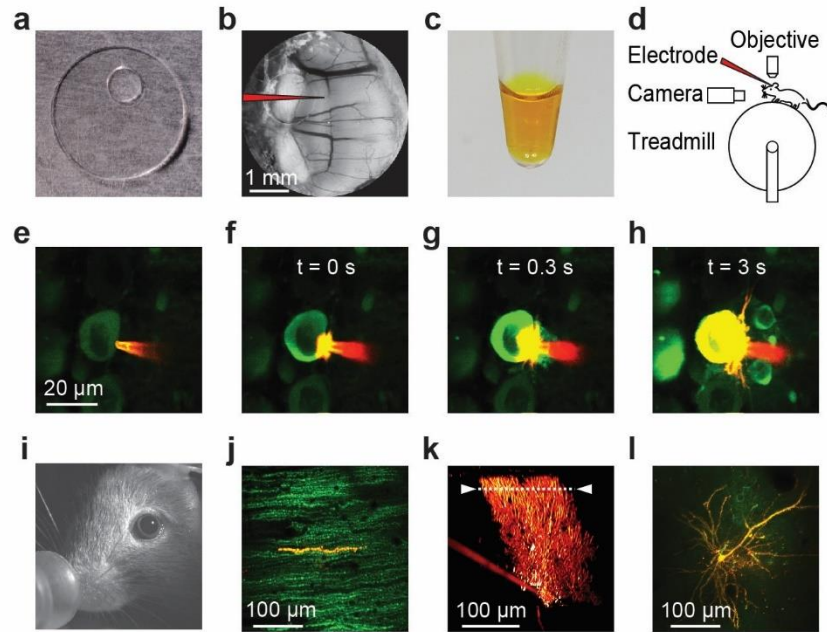
466 **Figure 1** Mechanism of voltage-sensitivity in electrochromic dyes. (a) Structure of three electrochromic
 467 dyes, ANNINE-6, ANNINE-6plus, and Di-4-ANEPPS. (b) Due to their hydrophobic and hydrophilic
 468 domains, electrochromic dyes bind to lipid membranes. (c) Excitation and emission of an electrochromic
 469 dye molecule causes a charge shift within the chromophore (center). This charge shift is modulated by an
 470 external electric field and shifts both the absorption and emission spectrum to either lower (left) or higher
 471 energy (right), corresponding to higher and lower wavelength, respectively. (Kuhn & Roome 2019)



473

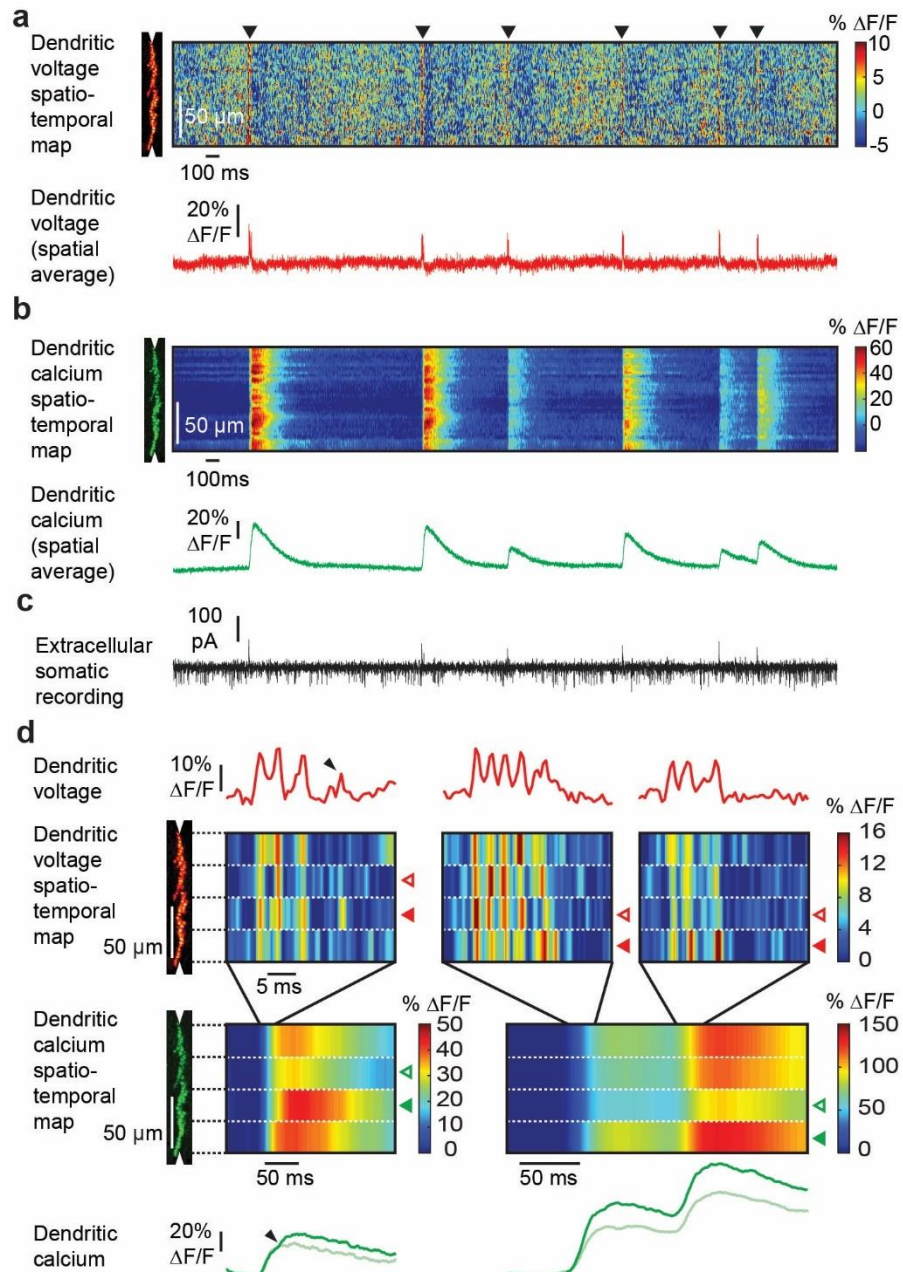
474 **Figure 2** Optimizing voltage imaging with a charge-shift probe by excitation at the red spectral edge of
 475 absorption, exemplified by ANNINE-6. (a) An external electric field shifts the excitation and the emission
 476 spectrum. In this example, the absorption spectrum of ANNINE-6 in the outer lipid membrane leaflet of a
 477 neuronal membrane at resting potential (black) is shifted by a 100 mV membrane voltage change (red),
 478 corresponding to an action potential. The spectral shift is about 3 nm. (b) The difference between the two
 479 spectra, the fluorescence change ΔF , shows a maximum and a minimum at the steepest slope of the
 480 spectrum. (c) The fluorescence change normalized by the spectrum at rest results in the relative fluores-
 481 cence change $\Delta F/F$. The relative fluorescence change diverges at the red spectral edge of absorption. If a white
 482 light source – i.e. the photon output is distributed over a wide spectral range – is used for voltage imaging
 483 experiments, the signal ΔF is optimized by exciting a range around the steepest spectral slope (blue arrows,
 484 excitation band of about 440 to 470 nm). The ΔF integral of this spectral range is proportional to the detected
 485 voltage signal. With laser excitation, however, it is possible to optimize the relative fluorescence change
 486 $\Delta F/F$ or sensitivity by excitation at the red spectral edge of the absorption spectrum (black arrows). $\Delta F/F$ is
 487 a measure of information gained per detected photon, and it rises steeply at the spectral edge. As the
 488 absorption cross-section in this spectral range is very low, practically infinitely bright light sources with

489 narrow spectral range, such as lasers, are required for this optimization to reach a sufficient intensity level
490 above photon shot-noise. Experimentally, the increase of sensitivity at the red spectral edge of absorption
491 can be shown with one-photon excitation (Kuhn et al 2004) and, here, two-photon excitation at twice the
492 excitation wavelength of one-photon excitation. (d,e) A HEK293 cell labeled with ANNINE-6 (f) is
493 exposed to external electric fields (field direction indicated by arrows in (d)) while scanning along the
494 membrane with two-photon excitation. (g) By increasing the excitation wavelength, the responses for the
495 same membrane voltage change get larger. The excitation power of the laser is increased to keep the
496 measured fluorescence intensity constant when exciting closer to red spectral edge of absorption. (h) The
497 responses are linear in the physiological range of membrane voltage changes. Modified with permission
498 from Elsevier (Kuhn et al 2004).



499

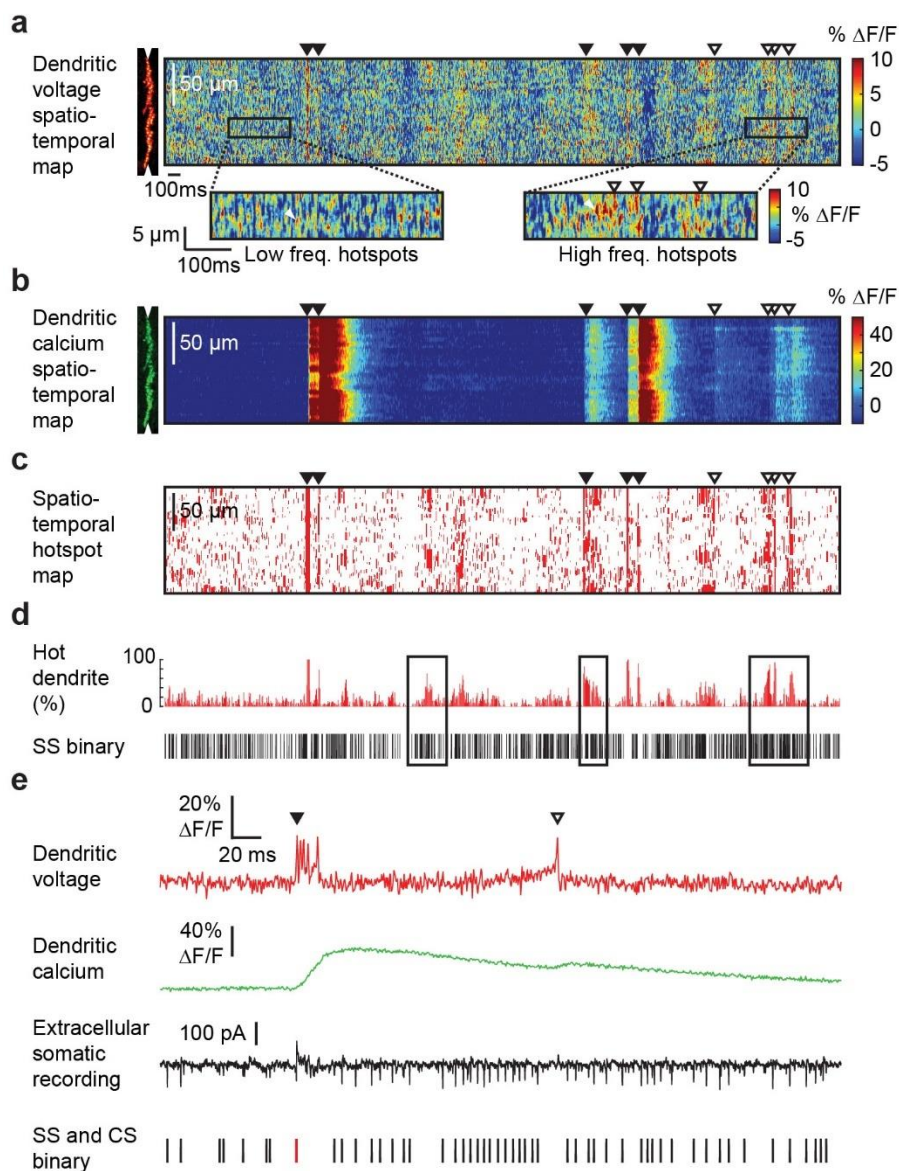
500 **Figure 3** Double-labelling individual neurons for combined voltage and calcium two-photon imaging in
 501 awake mice. (a) 5-mm glass cover slip with silicone access port (Roome & Kuhn 2014). (b) A chronic
 502 cranial window with access port on the vermis of the cerebellum allows access to the brain with a pipette
 503 (schematically indicated). (c) ANNINE-6plus dissolved in pure ethanol at 3 mM concentration. (d) Sketch
 504 of the setup with a mouse mounted on a treadmill under a two-photon microscope. An electrode is used to
 505 fill single neurons by electroporation and to electrically record from their soma. A behavioral camera allows
 506 detailed observation of the pupil, the vibrissa, and the face of the mouse. (e-h) A patch pipette filled with
 507 ANNINE-6plus/ethanol solution is used to label single GCaMP6f expressing neurons by electroporation in
 508 the anesthetized mouse. (i) During the imaging experiment the mouse is fully awake, sitting on a treadmill
 509 and monitored with behavioral a camera. 24 hours after labelling a Purkinje neuron with ANNINE-6plus,
 510 the dye has spread out evenly, as can be seen in (j) the cross section of the Purkinje neuron dendrite as an
 511 overlay of the green channel (GCaMP6f) and the red channel (ANNINE-6plus) and in (k) the reconstruction
 512 of the Purkinje neuron in the red channel (ANNINE-6plus). The dotted line indicates the line scan position
 513 used in Fig. 4 and 5. It is also possible to fill other neurons with ANNINE-6plus by electroporation, as, for
 514 example, (l) cortical layer 2/3 pyramidal neurons shown as overlaid z-projection of the green channel
 515 (GCaMP6f) and the red channel (ANNINE-6plus). (Roome & Kuhn 2019)



516

517 **Figure 4** Simultaneous voltage and calcium imaging of Purkinje neuron dendrites and somatic recording
 518 in the awake mouse. (a) A line scan at 2 kHz was taken along the Purkinje neuron dendrites (scan position
 519 shown in Fig. 3j) to record a voltage spatio-temporal map in an awake mouse. The spatially averaged
 520 dendritic voltage (red trace) clearly shows suprathreshold dendritic complex spikes (black triangles). (b)
 521 The corresponding dendritic calcium spatio-temporal map and spatially averaged dendritic calcium (green
 522 trace) shows large calcium transients for every dendritic complex spike. (c) The access port also allowed
 523 simultaneous extracellular electrical recordings from the soma (black trace) while imaging voltage and

524 calcium transients from the dendrites. Simple spikes (somatic Na⁺ spikes) result in a current sink at the
525 soma, while complex spikes (dendritic Ca²⁺ spikes) result in a dominant current source signal at the soma.
526 (d) Different parts of the dendritic tree show a different number of spikelets during the same complex spike
527 event. The number of spikelets correlate with the amplitude of the calcium transients in each part of the
528 dendritic tree. Open arrowheads indicate spatially localized low activity, filled arrowheads show high
529 activity. Spatially localized dendritic spikelets during complex spikes correlate with a local boost in the
530 dendritic calcium transient (small arrowheads). (Roome & Kuhn 2018)



532

533 **Figure 5** Sub- and suprathreshold dendritic signaling in awake mice. (a) Dendritic voltage spatio-temporal
 534 maps show epochs of low and high frequency subthreshold 'hotspot' events in Purkinje neuron dendrites
 535 (scan position shown in Fig. 3j). White arrow heads indicate single hotspot events. (b) The corresponding
 536 calcium spatio-temporal map does not show any correlated calcium transients except following
 537 suprathreshold complex spikes and dendritic spikes indicated in (a) by filled and open triangles,
 538 respectively. (c) By thresholding and additional spatio-temporal selection criteria, a spatio-temporal hotspot
 539 map can be generated. (d) Hotspot activity correlates with the simple spike (SS) activity at the soma. (e)
 540 Spatially averaged dendritic voltage (red) and calcium (green) recorded at 2kHz, reveal rapid (1-2 ms) and

541 variable suprathreshold dendritic spikelets during complex spikes (filled triangle). Extracellular somatic
542 recordings (black) were used to identify the somatic output signals; simple spikes (SS: black binary trace)
543 and complex spikes (CS: red binary trace). Non-climbing fiber evoked suprathreshold dendritic calcium
544 spikes (open triangles) were detected in the awake mouse which enhance local calcium influx and showed
545 no coincident sodium influx (simple spike) at the soma. (Roome & Kuhn 2018)